The Use of Satellite and Airborne Imagery to Inventory Outlet Glaciers of the Southern Patagonia Icefield, South America

M. Aniya, H. Sato, R. Naruse, P. Skvarca, and G. Casassa

Abstract

A Landsat TM mosaic of the Southern Patagonia Icefield (SPI), South America, was utilized as an image base map to inventory its outlet glaciers. The SPI is South America's largest ice mass with an area of approximately 13,000 km². The icefield does not have complete topographic map coverage. With the aid of stereoscopic interpretation of aerial photographs and digital enhancement of the Landsat TM image, glacier divides were located and glacier drainage basins were delineated, giving a total of 48 outlet glaciers. Employing a supervised classification using Landsat TM bands 1, 4, and 5, glacier drainage basins were further divided into accumulation and ablation areas, thereby determining the position of the transient snow line (TSL). After comparing with existing data, it was found that the TSL could be taken, for practical purposes, as the equilibrium line (EL). The position of the TSL was then compared with topographic maps, where available, to determine the equilibrium line altitude (ELA). Altogether, 11 parameters relating primarily to glacier morphology were inventoried. Pio XI Glacier (1265 km²) is found to be the largest outlet glacier in South America, and may also be its longest. The average accumulation area ratio of 0.75 is larger than those of the Northern Patagonia Icefield and European glaciers. All but two outlet glaciers calve into fjords or proglacial lakes.

Introduction

In light of recent, apparent global warming, it has become very important to monitor recent variations of glaciers, because their existence depends primarily upon precipitation and the air temperature of the region. In particular, the behavior of temperate glaciers (glaciers whose temperature is at the melting point throughout the glacier ice) is regarded to be indicative of climate changes, as they typically respond to such changes in a short period of time. In this context, the World Glacier Monitoring Service (WGMS, 1991) has initiated a program of worldwide monitoring of glacier variations (Haeberli, 1995). In the WGMS data set, it is natural that data from European glaciers are most abundant. Data from North America and some other populated regions are also available. Notably lacking in the list of this survey are data from Patagonian glaciers. The probable reasons include the following: (1) the region is sparsely inhabited, so local residents rarely observe the condition of the glaciers; (2) the region is located far from North America and Europe, where extensive glaciological studies have been carried out; (3) the interest of local scientists is relatively low; and (4) the icefields are remote, inaccessible, and plagued by persistent bad weather. The Patagonian icefields are important to the understanding of the trend of recent worldwide glacier variations, because they are in the Southern Hemisphere where land mass is scarce, they are located at the southern end of the Andes, they are one of the largest ice masses in the world, and they are the largest temperate ice mass in the Southern Hemisphere.

Two large icefields exist in Patagonia: the Northern Patagonia Icefield (NPI, or Hielo Patagónico Norte, 4200 km²) and the Southern Patagonia Icefield (SPI, or Hielo Patagónico Sur, 13000 km², Figure 1) (Mercer, 1967). In the NPI, Valdivia (1979) did a pioneering inventory of outlet glaciers. Aniya (1988) made a detailed inventory of outlet glaciers and elucidated the variations of these glaciers between 1944/45 and 1985/86, finding that most glaciers had been retreating at increased rates. For the SPI, Bertone (1960) compiled a simple glacier inventory using preliminary maps produced from Trimetrogon aerial photographs taken in 1944/45. In Bertone's work, however, he listed only those glaciers distributed in Argentina without a map showing their locations. In that inventory, glacier drainage basins were broken down into units of small tributary basins for which a few parameters were listed, so that for practical purposes it has been rarely referred to. Even today, reasonably reliable statistics on the drainage areas are available for only four glaciers (Naruse *et al.*, 1987; Aniya and Skvarca, 1992; Aniya and Sato, 1995), and topographic maps, even at a scale of 1:250,000, cover only a small part of the icefield. For such a region, remotely sensed data, particularly systematic, repetitive satellite image acquisition, seem to be well suited for glaciological studies. However, only a limited amount of sat-

M. Aniya is with the Institute of Geoscience, University of Tsukuba, Ibaraki 305, Japan.

H. Sato is with the Graduate School of Environmental Sciences, University of Tsukuba, Ibaraki 305, Japan (he is currently with PASCO, 2-13-5 Higashiyama, Meguroku, Tokyo 153, Japan).

R. Naruse is with the Institute of Low Temperature Science, Hokkaido University, Sapporo 060, Japan.

P. Skvarca is with the Glaciology Division, Instituto Antártico Argentino, Cerrito 1248, Buenos Aires, Argentina.

G. Casassa is with the Instituto de la Patagonia and Dirección de Programas Antárticos, Universidad de Magallanes, Punta Arenas, Chile.

Photogrammetric Engineering & Remote Sensing, Vol. 62, No. 12, December 1996, pp. 1361–1369.

0099-1112/96/6212–1361$3.00/0
© 1996 American Society for Photogrammetry and Remote Sensing

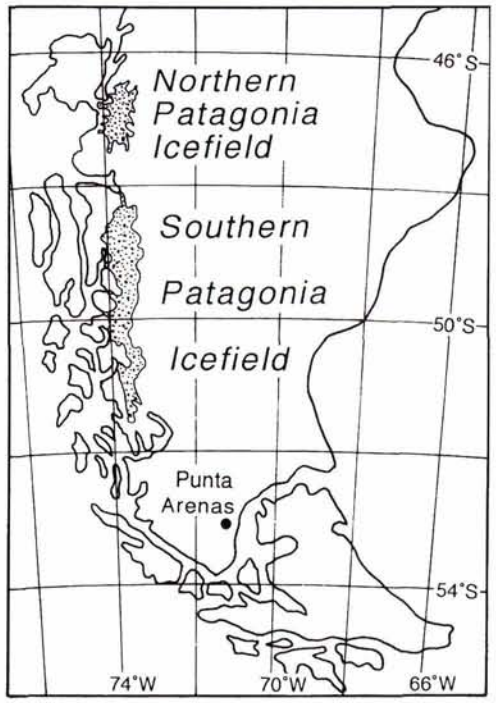

Figure 1. Study area: Southern Patagonia Icefield, South America.

ellite data are available for this region, because the weather conditions are exceptionally inclement due to its location in the westerlies belt known as the "roaring forties" and "furious fifties." For example, for the entire area of the icefield (three scenes), only one date (14 January 1986) of almost cloud-free images is available since the inception of the Landsat program in 1972. A few Landsat 2 and 3 multispectral scanner (MSS) and Landsat 3 Return Beam Vidicon (RBV) images are available for parts of the icefield that are suitable for glaciological analysis (Lliboutry, in press). Kotlyakov and his colleagues (Denisov *et al.*, 1987) used Salyut-6 space photographs of the SPI (especially 10 March 1978) to carry out a preliminary remote sensing study of several outlet glaciers including O'Higgins, Moreno, and Braggen [*sic.*, Brüggen or Pio XI] glaciers. Subsequently, Krimmel (1988) pointed out their misinterpretation of packed icebergs as the snout of O'Higgins Glacier, thereby revealing a problem in satellite glaciology. Utilizing this meager source of remotely sensed data, Aniya *et al.* (1992) and Aniya and Skvarca (1992) made studies on detailed variations of several glaciers since 1944/45. Recently Warren and Sugden (1993) made a survey of variations of 28 outlet glaciers from various sources, including remotely sensed data.

Although the study of the frontal variation itself of the glacier does not require information on the statistics of the glacier such as total area, equilibrium line altitude (ELA), and areas of accumulation and ablation, these data are important to interpret and comprehend the variation patterns of glaciers. Satellite data have been utilized in glaciology to detect, for example, glacier surface conditions (e.g., Williams, 1983; Hall and Ormsby, 1983; Orheim and Lucchitta, 1987; Hall *et al.*, 1987; Williams and Hall, 1993). Their advantage for compiling glacier inventories were also pointed out by Williams (1986) and they were utilized to delineate partial drainage divides of outlet glaciers of Vatnajökull (8300 km^2), Iceland (Williams, 1987). However, the application of satellite data to the compilation of a glacier inventory is still quite limited, although the World Glacier Monitoring Service (Scherler, 1983) provided guidelines for the preparation of preliminary glacier inventories using satellite data. In this study we present an inventory of outlet glaciers of the SPI, utilizing a Landsat TM mosaic of the area as the base map *in lieu* of topographic maps, complemented by other remotely sensed data and partially covering topographic maps.

Study Area — Southern Patagonia Icefield

The SPI extends for about 350 km between 48°20' and 51°30'S along 73°30'W. The width is generally 30 to 40 km, with the narrowest part only eight kilometres wide. The area in 1944/45 was 13,500 km^2 (Lliboutry, 1956), measured on preliminary maps at a scale of 1:250,000 produced from Trimetrogon aerial photographs taken by the U.S. Army Air Force, whereas it was 13,000 km^2 in 1986 (Naruse and Aniya, 1992), measured on a Landsat TM mosaic. Thus, the icefield area had shrunk by about 4 percent in 41 years, assuming that the 1:250,000-scale maps depicted accurately the areal extent of the SPI. In the SPI, although Warren and Sugden (1993) listed variations of 28 outlet glaciers since 1944/45, only several out of nearly 50 outlet glaciers have been studied in detail to determine variations since 1944/45 (Aniya *et al.*, 1992; Aniya and Skvarca, 1992). These findings indicate that most outlet glaciers have been retreating. However, there are a few glaciers whose behavior has been contrary, posing interesting problems as to the mechanism of glacier variations.

For example, Pio XI (also called Brüggen) Glacier, the largest outlet glacier in South America and located on the mid-west (wet) side of the icefield, had advanced about 9 km between 1944/45 and 1976 (290 m/yr), blocking a fjord, and its snout had split into two tongues. Comparison of Landsat images of 1976 and 1986 revealed that, while the northern tongue had continued to advance by 1200 m (120 m/yr), the southern tongue had retreated up to 600 m (60 m/yr) (Aniya *et al.*, 1992). This glacier is probably the only glacier in the world currently at its Neoglacial maximum (Warren and Rivera, 1994). The O'Higgins Glacier, only 60 km across the icefield to the northeast of Pio XI Glacier is located on the mid-east (dry) side of the SPI, calves into a freshwater lake. This glacier had retreated about 13.4 km (327 m/yr) between 1944/45 and 1986, by far the largest retreat in Patagonia. The accumulation fields of these two glaciers lie at similar latitudes, but under probably different precipitation regimes. About 120 km farther south, Upsala Glacier had retreated about 3 km between the early 1960s and 1990 (110 m/yr). However, additional remotely sensed data revealed that the middle part of the glacier had advanced up to 400 m between 1970 and 1978 (Aniya and Skvarca, 1992). The surface elevation near the snout had lowered by about 80 m between 1968 and 1990, and has lowered by 30 to 40 m during 1990-93 (11 m/yr) (Skvarca *et al.*, 1995). This lowering rate is one of the largest in the world.

Mosaicking and Geometric Correction of Landsat TM Images

Complete coverage of the SPI with Landsat TM images requires two-and-a-quarter consecutive scenes, and only those taken on 14 January 1986 (scene IDs: Y5068413530XO, Y5068413533XO, and Y5068413535XO from the north) are reasonably cloud-free for remote sensing applications to the entire SPI. After subsetting the area containing the icefield from the two and a quarter scenes, these scenes were mosaicked.

The Carta Preliminar at a scale of 1:250,000 is the only map series that covers the entire SPI. It was published by the Instituto Geográfico Militar of Chile from Trimetrogon aerial photographs taken by the U.S. Army Air Force during 1944/45. Although the hypsometric information on this map is not

reliable, the planimetric information appears reasonably correct, and this map series produced on the Lambert Conformal Conical Projection was used for geometric correction. Originally, 42 ground control points (GCP) were selected around the icefield for rectification; however, only 11 points were utilized for the final correction using a second-degree affine transformation with residuals to within two pixels (60 m). Resampling was done by the nearest-neighbor method with a pixel size of 30 m for the entire mosaic, enabling further detailed analyses of individual glaciers (Plate 1). Because the altitude of the SPI ranges up to around 3000 m, the relief displacement of a high peak/ridge may be large even on the TM images, a fact that affects the area measurements of the glacier drainage on the TM mosaic; however, no possible counter-measure could be taken without more precise topographic map coverage. Because the divides of the outlet glaciers in the icefield are often quite vague, unlike those of water streams, slight imprecision of the rectified image may not seriously affect the outcome of the measurements.

Delineation of Outlet-Glacier Drainages and Their Accumulation and Ablation Areas

Glacier Drainage

Although a false color composite of the TM mosaic of bands 1 (0.45 to 0.52 μm), 4 (0.76 to 0.90 μm), and 5 (1.55 to 1.75 μm) gives three-dimensional perception where relief is high, these data alone are naturally not sufficient to locate divides for all outlet glaciers with reasonable confidence. As a first step, we have utilized vertical aerial photographs at nominal scales of 1:60,000 to 70,000 taken by the Chilean Government between 1979 and 1984, and by the Argentinean Government in 1968, 1970, and 1981. This facilitated stereoscopic inspection of the concerned areas. Also, where topographic maps (1:250,000-, 1:100,000-, and 1:50,000-scale) on which the divides could be fairly precisely located were available, they were used as well. However, because the divide is a three-dimensional feature, stereoscopic inspection was most effective. Nonetheless, we had problems in locating the divide where topography is very gentle and subdued due to extensive ice, and for some glaciers we could not locate the divide with reasonable confidence. Because the Patagonia Icefield appears very white because of the presense of snow without nunataks, moraine bands, or other supraglacial debris that would enhance image contrast, even three-dimensional perception could not often be obtained for some glaciers. This occurred often in the northern half of the SPI, particularly for the divides between O'Higgins, Chico, and Viedma glaciers. The accumulation areas of these glaciers are called "Meseta de los cuatro glaciares," the plateau of four glaciers. For this kind of divide, it would be impossible to locate the divide even in the field by surface observation only. Long-range monitoring of flow-patterns of these glaciers with many stakes set up in the suspected area is required. In such areas, image enhancement of the TM image was also employed along with checking crevasses and flowline patterns on the aerial photographs, from which we could locate the lowermost limit for the divide of each glacier. Therefore, if we take lowermost limits of Viedma and Chico glaciers, it gives an uppermost limit for O'Higgins Glacier, and vice versa. Accordingly, we listed such areas with a maximum and a minimum. For the missing tip of Occidental Glacier in the TM image, we compensated with a SPOT HX image (1987), and the cloud-covered Viedma Glacier was studied with a SPOT HP image (1991). The determined divides were first drawn in by hand on enlarged prints of the TM image and, referring to those prints, the divides were then digitized onto the TM mosaic. Checking the uncertainty of the location of the divides on topographic maps, it was estimated that the determined divides are situated within 3 km of the true divides.

We identified 48 outlet glaciers (Figure 2) for the inventory. The primary criteria of outlet glaciers for inclusion in the inventory are contiguity to the icefield and size of the drainage basin. Those glaciers whose accumulation areas are situated on the slope of mountains that face away from the icefield were not included. Balmaceda and Snowy glaciers, located at the southern end of the SPI, originate from Cerro (Mount) Balmaceda, not from the icefield. Because Cerro Balmaceda is contiguous to the icefield, both glaciers are included in the inventory. The narrowest part of the SPI, between Mayo Glacier - HPS (Hielo Patagónico Sur) 28 Glacier and Europa Glacier - Spegazzini Glacier, contains no outlet glacier, because that region is mountainous. The mountain glaciers are small, and have areas generally less than 10 km^2. Other cirque and valley glaciers located near the margin of the icefield are also excluded on the basis of contiguity and size.

Accumulation and Ablation Areas

Two of the most basic glacier statistics are the areas of accumulation and ablation. The accumulation area is where the amount of snow accumulation exceeds the amount of snow and ice lost through melting and sublimation during a period of one budget year, thereby nourishing the glacier. The ablation area is where the annual amount of snow and ice lost through melting and sublimation exceeds the annual amount of snow accumulation. The position where the amounts of annual snow accumulation and ice melt are equal is called the equilibrium line (EL) (Østrem and Brugman, 1991). The position of the EL shifts year to year, depending upon weather conditions during a particular year. The elevation of the EL is called the equilibrium line altitude or ELA. Thus, the area above the ELA, or the accumulation area, is always covered with snow or, near the EL, superimposed ice, whereas the area down glacier from the ELA, the ablation area, is bare-ice at the end of the melt season. The accumulation area is further subdivided into zones of superimposed ice, slush, wet-snow, percolation, and dry-snow (Müller, 1962; Benson and Motyka, 1979; Williams *et al.*, 1991; Paterson, 1994).

With manual interpretation of large-scale, remotely sensed data, such as aerial photographs, the task of distinguishing the snow-covered surface and bare-ice surface can be done relatively easily with careful analysis of the glacier-surface conditions. The bare-ice surface has less reflectivity and may contain many supraglacial features such as streams, ponds, crevasses, moraines, ogive bands/waves, and the like, whereas, in the snow-covered area, the surface is white with high reflectivity and is smooth. However, the scale of a satellite image is usually too small to detect such minute features; so an analysis of the spectral signature of the surface is carried out. Several studies have shown that, with reflected infrared (Landsat MSS band 7, TM bands 4, 5, and 7), snow and ice can be discriminated (e.g., Østrem, 1975; Hall *et al.*, 1987; Orheim and Lucchitta, 1987; Hall *et al.*, 1995). The accumulation area and the ablation area can therefore be distinguished if the time of imaging is adequate, that is, late summer just before the new permanent snowfall (Williams, 1987; Williams *et al.*, 1991).

In the SPI, the position of the EL was estimated at three outlet glaciers — Upsala, Moreno, and Ameghino glaciers — from aerial photographs and topographic maps (Aniya and Skvarca, 1992; Aniya and Sato, 1995). Plate 2a shows Moreno Glacier (Landsat TM bands 1, 4, and 5) with the EL drawn in, indicating subtle changes in glacier-surface conditions near the EL. Using Moreno Glacier for field-based observations, the signatures of the bare-ice surface and the snow-covered surface of each band of the TM were examined. It was found out that, with band 4 (0.76 to 0.90 μm) alone, these two types of the surfaces could easily be distinguished,

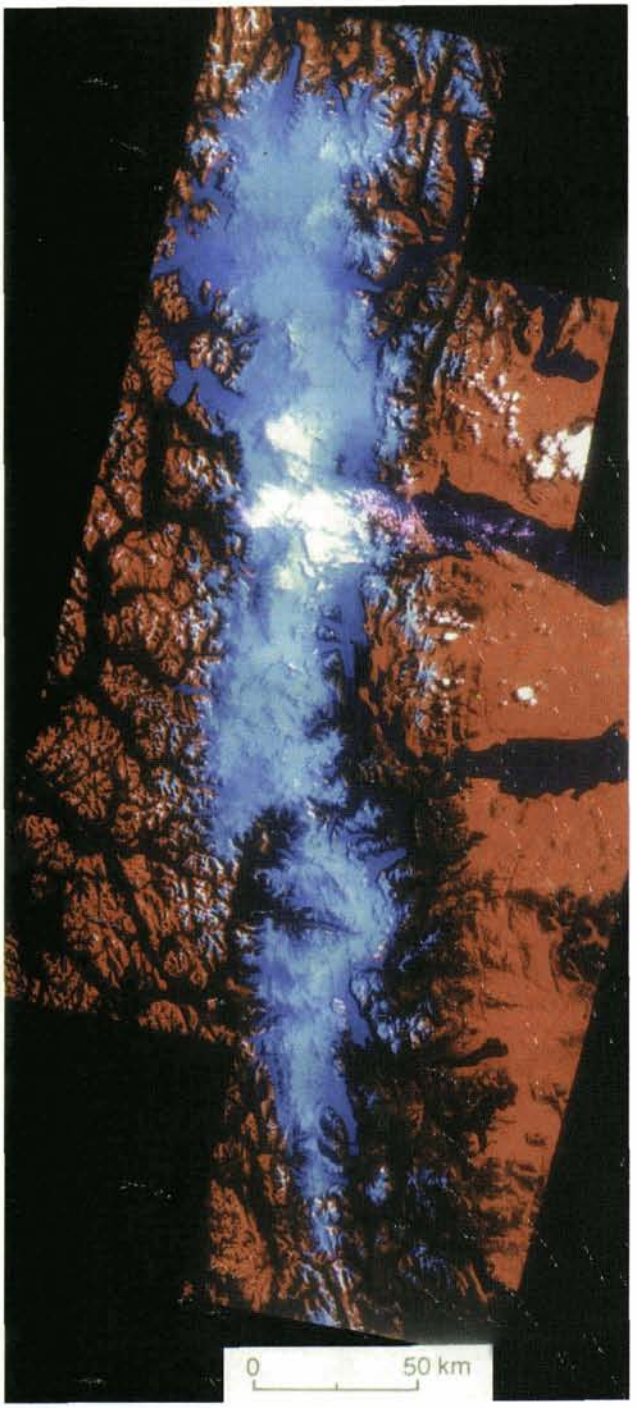

Plate 1. Landsat TM mosaic of the Southern Patagonia Icefield. The images were taken on 14 January 1986 (scene ID: Y5068413530XO, Y5068413533XO, Y5068413535XO). Two full and one 1/4 scenes were pieced together and geometric correction was applied using the Carta Preliminar of Chile (1:250,000 scale, Lambert Conformal Conic Projection). We used band 1 (0.45 to 0.52μm) with blue filter, band 2 (0.76 to 0.90μm) with green filter, and band 5 (1.55 to 1.75μm) with red filter to produce this false-color composite image. The area of the bluish tint stretching north-south along the central part is the icefield (snow and ice), the reddish area is bare rock/earth, and the greenish tint on the eastern side of the icefield is vegetated area. White patches over the central part of the icefield are clouds.

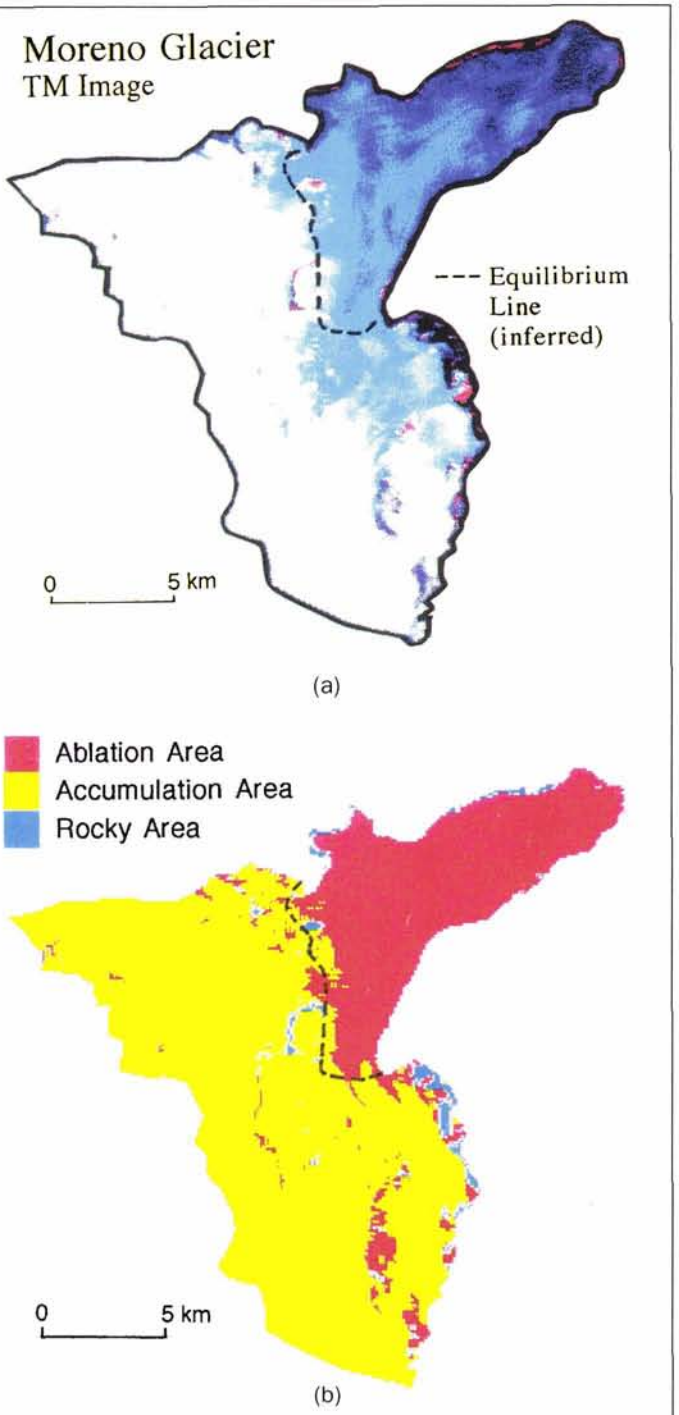

Plate 2. (a) Landsat TM false-color image (bands 1, 4, and 5, image ID Y5068413533XO) of Moreno Glacier with the equilibrium line (Aniya and Skvarca, 1992) drawn by hand. Subtle changes in glacier surface conditions near the EL are discernible, probably reflecting the size of snow grains and water content of snow and ice. (b) Spectral-analysis-based classification of Moreno Glacier, that groups 20 clusters (ISODATA) into classes of the accumulation, ablation, and exposed-bedrock areas. The spectral information from these data were utilized for the subsequent supervised classification of other glaciers. The parallel offset of the two ELs suggests that the discrepancy was probably caused by the time of image aquisition (image ID Y5068413533XO, 14 January 1986).

as well as the bedrock exposure to some extent, although Hall *et al.* (1987) used the ratio of band 4 to band 5 (1.55 to 1.75 μm). Using bands 1, 4, and 5, a cluster analysis (ISODATA) was applied to Moreno Glacier. With reference to the previously determined EL, 20 clusters were grouped into classes of the accumulation area, ablation area, and areas of bedrock exposures (Plate 2b). In Plate 2b, a slight difference in the EL position between those determined with the aid of aerial photographs and the cluster analysis of the satellite image was probably caused by the time of the image acquisition (14 January, mid-summer), reflecting the difference in grain size of snow or conditions such as wet or slushy snow (Choudhury and Chang, 1981; Dozier, 1984; Hall and Martinec, 1985; Williams, 1987; Williams *et al.*, 1991). However, it is regarded as a reasonable approximation. Subsequently, all pixels falling into each of the three classes of accumulation area, ablation area, and the area of bedrock exposures were used as training samples for the subsequent parallelepiped and maximum-likelihood classifications, and these spectral values were utilized to classify other glaciers into these three classes. The parallelepiped classification was primarily used as it was simple, and, when ambiguity was encountered, the maximum-likelihood classification was employed. Where misclassification was apparent, which was mostly the results of shadows, moraines, and other supraglacial debris on the glacier and snow surfaces, manual correction was applied before the classification was completed.

After separating the accumulation (snow only, not including superimposed ice) and ablation areas (glacier ice only, but may include superimposed ice which has similar reflectivity) and bedrock exposures, we measured each area by counting the number of pixels, each representing 900 m^2 (30 by 30 m). The total area was taken as the summation of accumulation and ablation areas, excluding bedrock exposures. A ratio of the accumulation area to the total area is called AAR (accumulation-area ratio), an index of the condition of the glacier's mass that can be used to compare glaciers in different regions.

In order to estimate the accuracy of the area measurements, the statistics of Upsala, Moreno, and Ameghino glaciers were compared with those measured on the topographic maps (Aniya and Skvarca, 1992; Aniya and Sato, 1995; Table 1). The discrepancy is up to 79 km^2, or 15 percent of the map measurement, for the accumulation area of Upsala Glacier. For Moreno and Ameghno glaciers, agreements are good. In general, the discrepancies in the areas of accumulation are prominent compared with the total areas. The satellite measurements of the accumulation areas are consistently more than the map measurements, an error introduced from the date of imaging (e.g., still too much snow cover). However, on the whole, the areas measured on the TM mosaic seem reasonably reliable, as indicated by the discrepancies for Moreno Glacier that was utilized for calibration of the spectral information, considering the type of the data, the nature of vague divides, and the method involved for locating the ELs. The large discrepancies at Upsala Glacier were probably caused largely by the relief displacement of 3000-m mountains delimiting the western divide. The ELs are also shown in Figure 2.

Another important parameter of the glacier is the equilibrium line altitude (ELA), that shifts up or down in response to climate changes. In order to obtain the ELA, we need information on the elevation that cannot usually be extracted from the satellite image alone. At 23 glaciers the EL on the TM mosaic could be compared with the topographic map to read the ELAs.

TABLE 1. COMPARISON OF THE AREA MEASUREMENTS ON THE LANDSAT TM MOSAIC WITH THOSE FROM TOPOGRAPHIC MAPS.

Glacier		Map Measurement (km^2)	TM Mosaic Measurement (km^2)	Difference (km^2)
Upsala	Total Area	857	901	+44
	Acc. Area	522	611	+79
	Abl. Area	325	290	−35
Moreno	Total Area	255	258	+3
	Acc. Area	180	188	+8
	Abl. Area	75	70	−5
Ameghino	Total Area	75	76	+1
	Acc. Area	31	32	+1
	Abl. Area	44	44	0

Map measurements of Upsala and Moreno Glaciers based on Aniya and Skvarca (1992) and those of Ameghino Glacier based on Aniya and Sato (1995); but from their measurements, the area of bedrock exposures in the accumulation area was subtracted (i.e., Upsala 13 km^2, Moreno 2 km^2, Ameghino 2 km^2), changing also the total area.

Glacier Inventory and Major Findings

After determining the glacier drainage divide, separating the accumulation area from the ablation area on the Landsat TM mosaic, and comparing the EL position with topographic maps, where possible, to establish the ELAs, we compiled the following glacier parameters for an inventory following the NPI example (Aniya, 1988): (1) location of the snout (as of 14 January 1986) in latitude and longitude, (2) length, (3) total area, (4) accumulation area and its aspect, (5) ablation area, (6) AAR, (7) ELA, (8) presence of calving (yes or no), (9) highest elevation, (10) lowest elevation (when calving into fjord, 0 m), and (11) relief (difference between parameters 9 and 10). Table 2 lists these parameters for each of the 48 outlet glaciers. In this table, for the total and accumulation areas, those including bedrock exposures are also indicated in parentheses, because steep bedrock exposures may contribute to the accumulation through snow and ice avalnches. Glacier names are primarily taken from Lliboutry (1956) except for a few glaciers whose names were adopted from Chilean topographic maps. These include Pascua Glacier (listed as Oriental Glacier on Lliboutry's map) and Oriental Glacier (which carries no name on Lliboutry's map). Mellizo Sur and Bravo glaciers are listed as Huemul and Rivera glaciers, respectively, on Lliboutry's map. On the other hand, Asia Glacier is listed as Brujo Glacier on a Chilean topographic map; but we used Asia. Occidental Glacier was called Hammick Glacier by Mercer (1970). The ELA could be estimated for 23 glaciers. The ELAs of other glaciers may be inferred from the estimated ELAs of neighboring glaciers. The area statistics of Upsala and Moreno glaciers are those measured on the Landsat TM mosaic, conforming to other data; however, the statistics measured on the topographic map should probably be regarded as correct. The total area of these outlet glaciers is about 11,260 km^2, with about 230 km^2 of bedrock exposures in the accumulation area. Therefore, about 1,510 km^2 of the total estimated area of 13,000 km^2 belongs to small valley and cirque glaciers found at the periphery of the icefield. From the inventory, we can summarize the following major characteristics of the SPI, many of which were hitherto unknown:

- Pio XI Glacier is the largest outlet glacier with an area of 1,265 km^2, which makes it also the largest in South America. This glacier may also be the longest at 64 km in length. Previously, Upsala Glacier was thought to be the largest with an area of 595 km^2 (Rabassa and Clapperton, 1990) or 870 km^2 (Aniya and Skvarca, 1992). The group of the second largest outlet glaciers consists of Upsala, Viedma, and O'Higgins glaciers, each with an area of around 900 km^2. The group of the third largest outlet glaciers includes Jorge Montt, Bernardo, and Penguin glaciers, each with an area of around 500 km^2. These large glaciers are located in the northern half of the

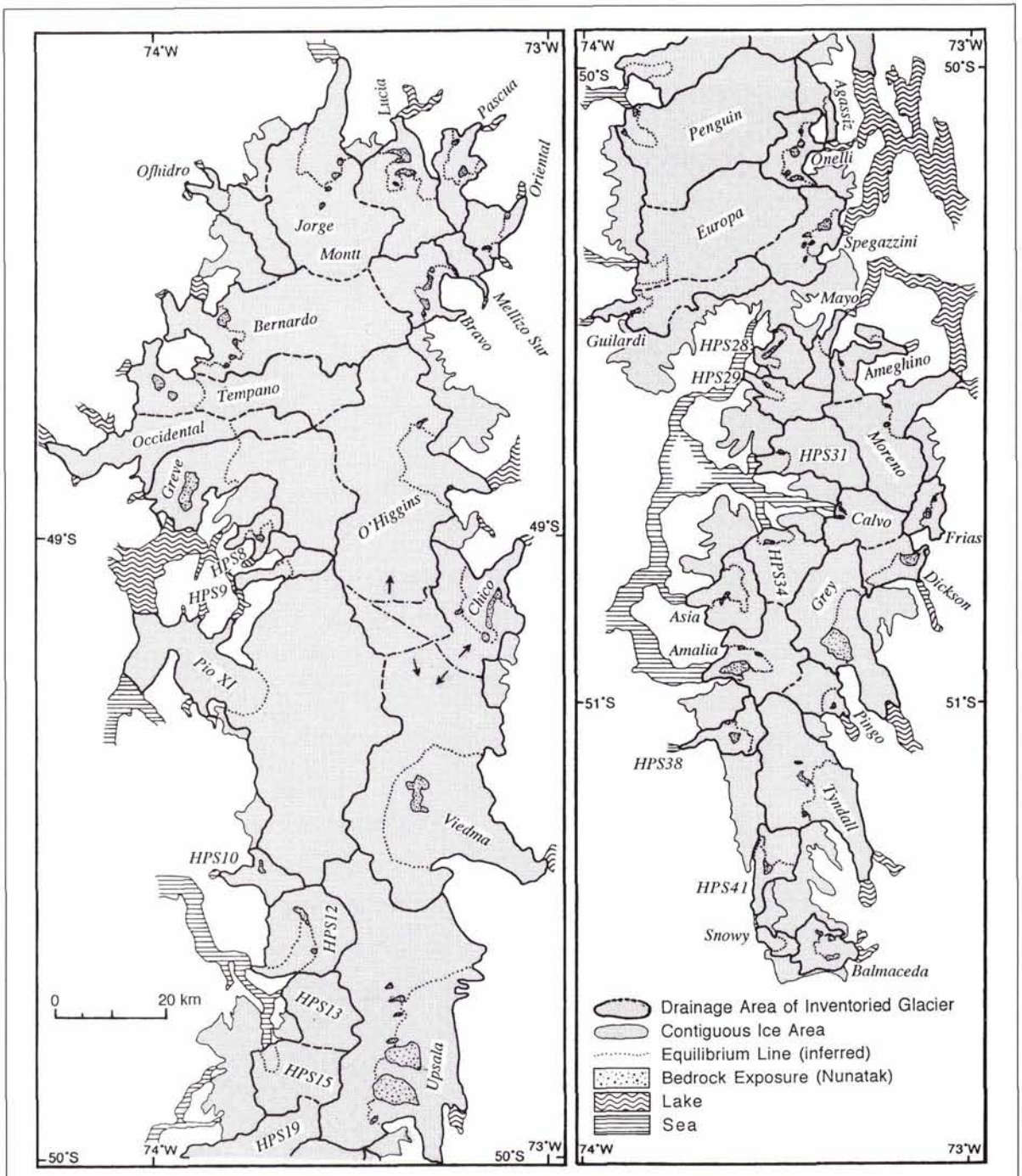

Figure 2. Glacier drainages and the equilibrium lines of outlet glaciers, determined from the Landsat TM mosaic (Plate 1) by remote-sensing techniques. The dashed lines indicate the inferred position of glacier divides. Contiguous ice areas (small cirque and valley glaciers, not inventoried) are delineated by a thin line. The divides between O'Higgins, Chico, and Viedma glaciers could not be determined because they are too subtle; however, dash-and-dot lines indicate the minimum limit of the divide for each of them. The maximum position for the divide of O'Higgins Glacier coincides with the minimum position for Viedma and Chico glaciers. The inferred maximum position of Viedma and Chico glaciers is shown with a dash-and-two dot line.

icefield, sharing their divides, suggesting less rugged subglacial topography of this area than the southern half.

- As for length, Viedma Glacier has a range of 71 to 55 km, depending upon the location of the divide. Pio XI and Upsala glaciers are more than 60 km long. Bernardo, Témpano, Occidental, and Greve glaciers, located in the northwestern part of the icefield, are about 50 km long.
- The average AAR of the individual glaciers is 0.72, with a range of 0.25 (Occidental Glacier) to 0.97 (Calvo Glacier): however, only eight outlet glaciers have an AAR less than 0.60. The SPI as a whole has an AAR of 0.75. The AAR of Occidental Glacier seems unusually small; the accumulation area lies on the windward side of the high, north-south-running divide of the icefield. Those glaciers on the west side of the

TABLE 2. INVENTORY OF THE SOUTHERN PATAGONIA ICEFIELD (BASED ON A LANDSAT TM MOSAIC, 14 JANUARY 1986)

Glacier*	Terminus Position Lat.(S)	Terminus Position Long.(W)	Length (km)	Total Area** (km²)	Accumulation area** (km²)	Accumulation area** Aspect	Ablation Area (km²)	AAR	ELA (m)	Calving Y or N	Highest Elev. (m)	Lowest Elev. (m)	Relief (m)
1 Jorge Montt	48° 04'	73° 30'	42	464(471)	348(355)	N	116	0.75	950	Y	2640	0	2640
2 Ofhidro	48° 25'	73° 51'	26	116(116)	91(91)	NW	25	0.79	1000	Y	1655	45	1610
3 Bernardo	48° 37'	73° 56'	51	536(541)	444(449)	W	92	0.83	1300	Y	2408	0	2408
4 Tempano	48° 44'	74° 03'	47	332(333)	242(243)	W	90	0.73	900	Y	2408	0	2408
5 Occidental	48° 51'	74° 14'	49	244(245)	60(61)	W	184	0.25	950	Y	—	<100	—
6 Greve	48° 58'	73° 55'	51	438(439)	292(293)	NW~W	146	0.67	1000	Y	3380	—	—
7 HPS8	49° 02'	73° 47'	11	38(40)	25(27)	SE	13	0.66	—	Y	—	—	—
8 HPS9	49° 03'	73° 48'	19	55(57)	29(31)	W	26	0.52	—	Y	3380	—	—
9 Pio XI	49° 13'	74° 00'	64	1265(1275)	1014(1024)	W	251	0.80	—	Y	3380	0	3380
10 HPS10***	49° 32'	73° 48'	16	61	—	W	—	—	—	Y	—	—	—
11 HPS12	49° 41'	73° 45'	23	204(212)	164(172)	S~W	40	0.80	—	Y	2257	0	2257
12 HPS13***	49° 43'	73° 40'	19	141	—	W	—	—	—	Y	2656	0	2656
13 HPS15	49° 48'	73° 42'	19	174(175)	164(165)	N~W	10	0.94	—	Y	2446	0	2446
14 HPS19	50° 00'	73° 55'	26	176(177)	157(158)	W	19	0.89	—	Y	—	0	—
15 Penguin	50° 05'	73° 55'	38	527(530)	507(510)	NW	20	0.96	—	Y	3180	0	3180
16 Europa	50° 18'	73° 52'	39	403(409)	379(385)	W	24	0.94	—	Y	—	0	—
17 Guilardi	50° 23'	73° 57'	36	148(151)	125(128)	W	23	0.85	—	Y	—	0	—
18 HPS28	50° 25'	73° 35'	12	63(68)	47(52)	W	16	0.75	—	Y	2238	0	2238
19 HPS29	50° 28'	73° 36'	17	82(84)	69(71)	W	13	0.85	1200	Y	2950	0	2950
20 HPS31	50° 36'	73° 33'	23	161(165)	141(145)	S~W	20	0.88	900	Y	2950	0	2950
21 Calvo	50° 41'	73° 21'	13	117(121)	114(118)	W	3	0.97	—	Y	—	0	—
22 HPS34	50° 43'	73° 32'	14	137(138)	122(123)	NW	15	0.89	800	Y	—	0	—
23 Asia	50° 49'	73° 44'	12	133(133)	86(86)	W	47	0.65	—	Y	2179	0	2179
24 Amalia	50° 57'	73° 45'	21	157(161)	126(130)	W	32	0.80	900	Y	—	0	—
25 HPS38	51° 03'	73° 45'	16	62(64)	27(29)	W	35	0.44	—	Y	—	—	—
26 HPS41	51° 18'	73° 34'	17	71(75)	39(43)	SW	32	0.55	—	Y	—	—	—
27 Snowy	51° 22'	73° 34'	9	23(24)	11(12)	W	12	0.48	—	Y	—	—	—
28 Balmaceda	51° 23'	73° 18'	12	63(69)	42(48)	E	21	0.67	650	Y	—	—	—
29 Tyndall	51° 15'	73° 15'	32	331(337)	213(219)	E	118	0.64	900	Y	—	50	—
30 Pingo	51° 02'	73° 21'	11	71(73)	56(58)	SE	15	0.79	—	Y	—	200	—
31 Grey	51° 01'	73° 12'	28	269(277)	167(175)	SE	103	0.62	—	Y	—	100	—
32 Dickson	50° 47'	73° 09'	10	71(77)	42(48)	SE	29	0.59	—	Y	—	—	—
33 Frias	50° 45'	75° 05'	9	48(51)	30(33)	E	18	0.62	—	N	—	—	—
34 Moreno#	50° 30'	73° 00'	30	258(265)	188(195)	NE	70	0.73	1150	Y	2950	175	2775
35 Ameghino##	50° 25'	73° 10'	21	76(77)	32(33)	N	44	0.42	1000	Y	2250	201	2049
36 Mayo	50° 22'	73° 20'	15	45(47)	28(30)	N~S	17	0.62	900	Y	2250	200	2050
37 Spegazzini	50° 15'	73° 20'	17	137(145)	116(124)	E~S	21	0.85	—	Y	—	175	—
38 Onelli	50° 07'	73° 25'	13	84(90)	52(58)	NE~S	32	0.62	—	Y	2940	175	2765
39 Agassiz	50° 06'	73° 22'	17	50(51)	37(38)	E	13	0.74	—	Y	3064	175	2889
40 Upsala###	49° 59'	73° 17'	60	902(929)	611(638)	SE	290	0.68	1150	Y	3180	175	3005
41 Viedma^	49° 31'	73° 01'	71~55	945~862 (964~881)	564~481 (583~500)	E~S	381	0.60~0.56	1250	Y	—	250	—
42 *Chico*^	49° 00'	73° 04'	38~25	306~243 (320~255)	257~194 (271~206)	E	49	0.84~0.80	—	Y	—	285	—
43 O'Higgins^	48° 55'	73° 08'	46~38	893~747 (902~754)	784~638 (793~645)	N~E~S	109	0.88~0.85	1300	Y	3380	285	3095
44 Bravo	48° 38'	73° 10'	23	129(134)	98(103)	E	31	0.76	1500	N	3067	300	2767
45 Mellizo Sur	48° 37'	73° 07'	14	37(44)	32(39)	SE	5	0.86	1400	Y	3067	300	2767
46 Oriental	48° 27'	73° 01'	17	74(77)	56(59)	E	18	0.75	1150	Y	3017	285	2732
47 Pascua	48° 22'	73° 09'	23	88(91)	58(61)	N	30	0.66	950	Y	3017	151	2866
48 Lucia	48° 20'	73° 20'	29	200(209)	145(154)	N	55	0.72	1000	Y	3067	27	3040
Total				11259 (11487)	8285^^ (8513)		2773^^	0.75^^					

*Glaciers are listed counter-clockwise from the north.

**Total area and accumulation area are listed without bedrock exposures: however, for additional information, those including bedrock exposures are also indicated in parentheses. For HPS10 and HPS13, bedrock exposures could not be located due to cloud cover.

***The equilibrium line could not be located due to cloud cover.

#The map measurements: total area 255 (257) km²; accumulation area 180 (182) km²; and ablation area 75 km² (Aniya and Skvarca, 1992, modified).

##The map measurements: total area 75 (77) km²; accumulation area 31 (33) km²; and ablation area 44 km² (Aniya and Sato, 1995, modified).

###The map measurements: total area 857 (870) km²; accumulation area 522 (535) km²; and ablation area 325 km² (Aniya and Skvarca, 1992, modified).

^The divide between these three glaciers could not be located with reasonable confidence; hence the minima and maxima are listed. Two square kilometers of bedrock exposures exist in the accumulation area that belongs either to O'Higgins or Chico glacier.

^^Total of 46 glaciers (not including HPS10 and HPS13).

icefield have an average of 0.75, while those on the east side have an average of 0.70. Four outlet glaciers have AARs exceeding 0.9, all on the west side of the southern half with calving fronts in fjords. The average AAR of 0.75 is considerably higher than that of the Northern Patagonia Icefield with 0.63 (Aniya, 1988) and much higher than European mountain glaciers with values less than 0.60 (e.g., Haeberli, 1995).

- The ELA ranges from 650 m at the southern end to 1500 m at the northeast end. In general, outlet glaciers located in the southern part have the ELAs below 1000 m, while those located in the northeastern sector have higher ELAs. This distribution pattern can probably be explained by the latitudinal difference and the east-west contrast in the climate (Warren and Sugden, 1993).
- One of the notable characteristics of the SPI outlet glaciers is that, except for two glaciers (Frias Glacier on the southeast and Bravo Glacier on the northeast), all glaciers are calving. Glaciers on the west calve mostly into fjords and those on the east into proglacial lakes. Particularly, Calvo, HPS34, Europa, Penguins, HPS19, HPS15, HPS13, and HPS12 glaciers are calving heavily so that fjords are packed with icebergs. These glaciers have exceptionally large AARs, all above 0.80. Thus, calving is very important as a dominant ablation process in Patagonia, resulting in short-term glacier variations being only indirectly related to climate changes (Warren, 1993; Warren and Rivera, 1994; Warren *et al.*, 1995).

The advantage of utilizing satellite image data, along with other remotely sensed and ancillary data, for inventorying glaciers in a remote, large area where map coverage is poor has been demonstrated for glaciological studies. By combining glacier characteristics revealed by this inventory and the trend of recent glacier variations, we can analyze the possible causes of the variations related to glacier dynamics, and possibly even to climatic forcing.

Acknowledgments

Mr. Andrés Rivera, Department of Geography, University of Chile, helped us obtain recently published Chilean topographic maps for this study. Detailed comments made by Dr. Richard S. Williams, Jr., of the U.S. Geological Survey; Dr. Charles R. Warren, School of Geography and Geology, University of St. Andrews, Scotland; and an anonymous reviewer helped improve the manuscript. We are grateful to Dr. Williams who made some literature available.

References

Aniya, M., 1988. Glacier inventory for the Northern Patagonia Icefield, Chile, and variations 1944/45 to 1985/86, *Arctic and Alpine Research*, 20:179–187.

Aniya, M., and P. Skvarca, 1992. Characteristics and variations of Upsala and Moreno glaciers, southern Patagonia, *Bulletin of Glacier Research*, 10:39–53.

Aniya, M., R. Naruse, M. Shizukuishi, P. Skvarca, and G. Casassa, 1992. Monitoring recent glacier variations in the Southern Patagonia Icefield, utilizing remote sensing data, *International Archives of Photogrammetry and Remote Sensing*, 29(B7):87–94.

Aniya, M., and H. Sato, 1995. Morphology of Ameghino Glacier and landforms of Ameghino Valley, southern Patagonia, *Bulletin of Glacier Research*, 13:69–82.

Benson, C.S., and R. Motyka, 1979. Glacier-volcano interactions on Mt. Wrangell, Alaska, *Annual Report 1977–78, Geophysical Institute, University of Alaska*, pp. 1–25.

Bertone, M., 1960. *Inventario de los glaciares: existentes en la vertiente Argentian entre los paralelos 47°30' y 51° S*, Instituto Nacional del Hielo Continental Patagónico, Ministerio de Educación y Justica de la Nación, Publicación No. 3, Buenos Aires, 101 p.

Choudhury, B.J., and A.T.C. Chang, 1981. On the angular variation of solar reflectance of snow, *Journal of Geophysical Research*, 86(C1):465–472.

Denisov, L.V., G.A. Nosenko, G.M. Grechko, A.S. Ivanchenko, and V.M. Kotlyakov, 1987. Glaciological studies and experiments from the Salyut-6 orbital space station, *Polar Geography and Geology*, 11:12–24.

Dozier, J., 1984. Snow reflectance from LANDSAT-4 Thematic Mapper, *IEEE Transactions on Geoscience and Remote Sensing*, GE-22(3):323–328.

Haeberli, W., 1995. Glacier fluctuatons and climate change detection — operational elements of a worldwide monitoring strategy, *Bulletin, World Meteorological Organization*, 44(1):23–31.

Hall, D.K., and J.P. Ormsby, 1983. Use of SEASAT synthetic aperture radar and LANDSAT multispectral scanner subsytem data for Alaskan glaciology studies, *Journal of Geophysical Research*, 88(C3):1597–1607.

Hall, D.K., and J. Martinec, 1985. *Remote Sensing of Ice and Snow*, Chapman and Hall, London, 189 p.

Hall, D.K., J.P. Ormsby, R.A. Bindschadler, and H. Siddalingaiah, 1987. Characterization of snow and ice reflectance zones on glaciers using Landsat Thematic Mapper data, *Annals of Glaciology*, 9:104–108.

Hall, D.K., R.S. Williams, Jr., and O. Sigurdsson, 1995. Glaciological observations of Brúarjökull, Iceland, using synthetic aperture radar and thematic mapper satellite data, *Annals of Glaciology*, 21:271–276.

Krimmel, R.M., 1988. Terminus of Glaciar O'Higgins, southern Chile, *Journal of Glaciology*, 34(116):142.

Lliboutry, L., 1956. *Nieves y Glaciares de Chile: Fundamentos de Glaciología*, Ediciones de la Universidad de Chile, Santiago, 471 p.

———, in press. Glaciers of Chile and Argentina (I-6), *Satellite Image Atlas of Glaciers of the World* (R.S. Williams, Jr., and J.G. Ferrigno, editors), U.S. Geological Survery Professional Paper 1386-I (Glaciers of South America).

Mercer, J.H., 1967. Glaciers of Chile and Argentina between latitude 46° S and the Straits of Magellan, in *Southern Hemisphere Glacier Atlas*, Technical Report 67-76-ES by the American Geographical Society, New York, for the Earth Sciences Laboratory, U.S. Army Natick Laboratories, Natick, Massachusetts, Series ES-33, June, pp. 131–154.

———, 1970. Variations of some Patagonian glaciers since the Late-Glacial: II, *American Journal of Science*, 269:1–25.

Müller, F., 1962. Zonation in the accumulation area of the glaciers of Axel Heiberg Island, N.W.T., Canada, *Journal of Glaciology*, 4(23):302–311.

Naruse, R., H. Peña, M. Aniya, and J. Inoue, 1987. Flow and surface structure of Tyndall Glacier, the Southern Patagonia Icefield, *Bulletin of Glacier Research*, 4:133–140.

Naruse, R., and M. Aniya, 1992. Outline of Glacier Research Project in Patagonia, 1990. *Bulletin of Glacier Research*, 10:31–38.

Orheim, O., and B.K. Lucchitta, 1987. Snow and ice studies by thematic mapper and multispectral scanner Landsat images, *Annals of Glaciology*, 9:109–118.

Østrem, G., 1975. ERTS data in glaciology — an effort to monitor glacier mass balance from satellite imagery, *Journal of Glaciology*, 15(73):403–414.

Østrem, G., and M. Brugman, 1991. *Glacier Mass-Balance Measurements: A Manual for Field and Office Work*, Environmental Canada, National Hydrology Research Institute, NHRI Science Report No. 4, 224 p.

Paterson, W.S.B., 1994. *The Physics of Glaciers*, 3rd ed., Pergamon Press, Oxford, 480 p.

Rabassa, J., and C.M. Clapperton, 1990. Quaternary glaciations of the southern Andes, *Quaternary Science Reviews*, 9:153–174.

Scherler, K.E., 1983. *Guidelines for Preliminary Glacier Inventories*, Temporary Technical Secretariat for the World Glacier Inventory, Glocal Environment Monitoring System, United Nations Environmental Programme, UNESCO, 16 p.

Skvarca, P., K. Satow, R. Naruse, and J. Leiva, 1995. Recent thinning, retreat and flow of Upsala Glacier, Patagonia, *Bulletin of Glacier Research*, 13:11–20.

Valdivia, P., 1979. *The North Patagonia Icefield, Glacier Inventory*, Temporary Technical Secretariat for World Glacier Inventory (UNESCO), 1L-6L, 1R-6R.

Warren, C.R., 1993. Rapid recent fluctuations of the calving San Rafael Glacier, Chilean Patagonia: Climatic or non-climatic? *Geografiska Annaler*, 75A(3):111–125.

Warren, C.R., and D.E. Sugden, 1993. The Patagonian Icefields: A glaciological review, *Arctic and Alpine Research*, 25(4):316–331.

Warren, C.R., and A. Rivera, 1994. Non-linear response of calving glaciers: a case study of Pio XI Glacier, *Revista Chilena de Historia Natural*, 67(4):385–394.

Warren, C.R., D.R. Greene, and N.F. Glasser, 1995. Upsala Glacier, Patagonia: Rapid calving retreat in freshwater, *Annals of Glaciology*, 21:311–316.

Williams, R.S., Jr., 1983. Remote sensing of glaciers, *Manual of Remote Sensing. Geological Appications*, 2nd Edition (R.N. Colwell, editor), American Society for Photogrammetry and Remote Sensing, Falls Church, Virginia, pp. 1852–1866.

———, 1986. Glacier inventories of Iceland: Evaluation and use of sources of data, *Annals of Glaciology*, 8:184–191.

———, 1987. Satellite remote sensing of Vatnajökull, Iceland, *Annals of Glaciology*, 9:127–135.

Williams, R.S., Jr., D.K. Hall, and C.S. Benson, 1991. Analysis of glacier facies using satellite techniques, *Journal of Glaciology*, 37(125):120–128.

Williams, R.S., Jr., and D.K. Hall, 1993. Glaciers, *Atlas of Satellite Observations Related to Global Change* (R.J. Gurney, J.L. Foster, and C.L. Parkingson, editors), Cambridge University Press, pp. 401–422.

World Glacier Monitoring Service, 1991. *Glacier Mass Balance Bulletin, Bulletin No. 1 (1988–1989)* (W. Haeberli and E. Herren, editors), IAHS (ICSI)-UNEP-UNESCO, 70 p.

(Received 13 June 1995; accepted 3 October 1995; revised 12 December 1995)

REPRINTS REPRINTS REPRINTS

Order reprints of any article published in ASPRS publications– Listed below are several of the ASPRS resources in our Libary.

Cost is $1/page plus postage– Faxes are $.25/page additional.

Limited quantities of off-prints with color covers available *(prices include first class postage)*:

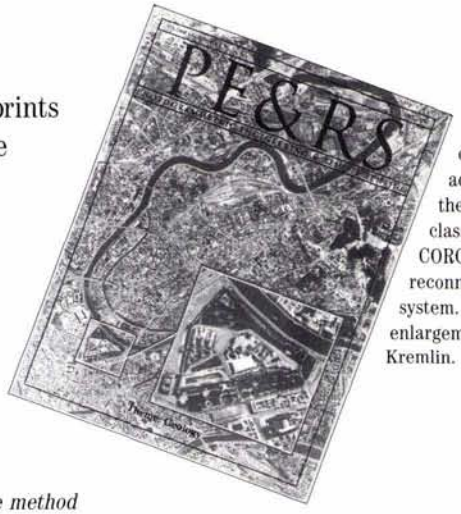

1970 scene of Moscow acquired by the formerly classified CORONA satellite reconnaissance system. Inset shows enlargement of the Kremlin.

- CORONA: Success for Space Reconnaissance, A Look into the Cold War, and a Revolution for Intelligence, 32pp, color–$7.50/ea
- Opening the Cold War Sky to the Public: Declassifying Satellite Reconnaissance Imagery, 6pp, B&W– $2/ea
- A New Tool for Depth Perception of Multi-Source Data *(describes the method to generate color composite images from multisource data in which depth perception is coded into color)*, 3pp, color– $2/ea

Reprints are available from all publications in the ASPRS library, including–

PE&RS

1934 to present
Partial listing of *PE&RS* Special Issues includes:
GIS/LIS
Softcopy Photogrammetry
Remote Sensing in Solid and Hazardous Waste Management
NASA Remote Sensing Applications
Plus every Annual Directory of the Mapping Sciences and
Annual Subject & Author Indices

MANUALS

Photogrammetry, all editions
Remote Sensing, all editions
Non-Topo. Photogrammetry, all eds.
Color Aerial photography, 1968

PROCEEDINGS

GIS/LIS, 1986-1995
AutoCarto, 1974-1995
Color Aerial Photography, 1967-1994
Pecora, 1975-1995
ISPRS Archives, 1952-1992
Close-Range Photogrammetry
...and much more

Send your order to:
ASPRS, Carolyn Staab
5410 Grosvenor Lane, Suite 210
Bethesda, MD 20814-2160
301-493-0290 fax 301-493-0208
cstaab@asprs.org